Emittance of a field emission electron source

K. L. Jensen,[1,a)] P. G. O'Shea,[2] D. W. Feldman,[2] and J. L. Shaw[1]
[1]*Code 6843, Electronic Science and Technology Division, Naval Research Laboratory, 4555 Overlook Avenue SW, Washington, DC 20375-5347, USA*
[2]*Institute for Research in Electronics and Applied Physics, Energy Research Facility, Bldg. #223, Paint Branch Drive, University of Maryland, College Park, MD 20742-3511, USA*

(Received 28 April 2009; accepted 2 November 2009; published online 5 January 2010)

An analytical formula of the emittance of a field emitter is given. In contrast to thermal and photoemission, such a formula contains complexity due to the multidimensional nature of the source. A formulation of emittance is given for one- and three-dimensional (3D) field emitters. The 3D formulation makes use of the point charge model of a unit cell emitter coupled with a trajectory analysis to follow electrons to an evaluation plane where emittance is determined. The single tip theory is extended to an array and the resulting theory predicts the emittance of a Spindt-type square array of emitters 0.2 cm on a side producing 2000 A/cm^2 is 23 mm mrad. Theory compares favorably with experimental measurements in the literature from ungated and gated sources. The impacts of several complications are estimated: the effects of a gate for modulating the emitter; the influence of space charge within the unit cell on the beam; and constraints imposed by modulation frequency, emitter dimensions, and rise/fall time requirements for turning a beam on and off, as determined by the array's *RLC* characterization. © *2010 American Institute of Physics*.
[doi:10.1063/1.3267288]

INTRODUCTION

Emittance is a figure of merit for judging the quality of an electron beam and is increasingly important as larger currents are confined to smaller areas. It refers to the tendency of a beam of particles to spread in cross section as the beam propagates and is given by the product of the beam size and its divergence. The emittance due to the cathode itself cannot be undone with subsequent beam manipulations ("beam optics") and therefore knowledge of the cathode emittance for various electron source technologies is important. Estimates of the emittance of a thermal emitter and a photoemitter exist in the literature. It is the purpose of this work to provide an account of field emission sources and is motivated by applications that seek high brightness electron sources. Such applications include but are not limited to advanced particle accelerators and free electron lasers (FELs),[1] millimeter-wave vacuum electronic (VE) amplifiers and terahertz devices,[2,3] electron beam lithography,[4,5] transmission electron microscopes,[6] and others.

In particular, for FELs, the electron beam must be focused within the laser beam optical mode within the wiggler in order for the laser threshold to be reached. The mode is characterized by a waist radius w and a divergence θ, the product of which is proportional to the wavelength of the device, or $w\theta = \lambda/\pi$. The waist-divergence product, or "emittance," must be such that the beam resides within the optical mode. Past FELs were operated at wavelengths of tens of microns, and so the emittance of the electron source could be large. In contrast, recent FELs seek to operate at a micron scale or smaller (for an x-ray FEL, much smaller) and so the emittance must be smaller.

For micro- and millimeter-wave power amplifiers that use thermionic cathodes, requiring the sources to produce a current density characteristic of that in the beam tunnel would render the lifetime of the dispenser cathode unacceptably short[7] and therefore the beam transverse dimensions are compressed after emission. Compared to an ideal or zero-emittance beam $J(\varepsilon=0)$, the current density $J(\varepsilon)$ in the beam tunnel is smaller by a factor that depends on beam R_b radius, magnetic field strength B, accelerating voltage V_b, frequency f (inversely related to R_b), harmonic number n, and emittance ε via $1-[J(\varepsilon)/J(0)] \propto (nf\varepsilon/R_bB)^2V_b$. B and V_b are constrained by technology and platform, higher frequency applications are desired, and higher harmonics may be sought. Cathode dimensions for past microwave amplifiers were large, but as the "power density" performance metric (the product of the power and frequency squared) has climbed, the dimensions of the beam tunnel have shrunk, and so a reduction in emittance is needed.

Here, a methodology to evaluate the emittance of field emission sources is developed. Field emitters have sharp apexes, therefore the usual one-dimensional (1D) methods used by thermal and photoemission theory require an expanded account to treat curved emitters in order to follow electron trajectories to an evaluation plane in which ε is calculated. A point charge model is provided to treat rotationally symmetric three-dimensional (3D) structures. The effect of combining single emitters into arrays on overall emittance is shown. Complications such as gating and space charge are considered. Finally, the modulation of actual field emitter array (FEA) sources is constrained by layout, tip geometry, and modulation frequency, and the consequences on how the arrays are operated to produce bunched beams is described. The reader is cautioned that conventions in the literature (and

a)Electronic mail: kevin.jensen@nrl.navy.mil.

Report Documentation Page

Form Approved
OMB No. 0704-0188

1. REPORT DATE	2. REPORT TYPE	3. DATES COVERED
APR 2009		**00-00-2009 to 00-00-2009**

4. TITLE AND SUBTITLE	5a. CONTRACT NUMBER
Emittance of a field emission electron source	5b. GRANT NUMBER
	5c. PROGRAM ELEMENT NUMBER
6. AUTHOR(S)	5d. PROJECT NUMBER
	5e. TASK NUMBER
	5f. WORK UNIT NUMBER
7. PERFORMING ORGANIZATION NAME(S) AND ADDRESS(ES) **Naval Research Laboratory,Code 6843, Electronic Science and Technology Division,4555 Overlook Avenue SW,Washington,DC,20375**	8. PERFORMING ORGANIZATION REPORT NUMBER
9. SPONSORING/MONITORING AGENCY NAME(S) AND ADDRESS(ES)	10. SPONSOR/MONITOR'S ACRONYM(S)
	11. SPONSOR/MONITOR'S REPORT NUMBER(S)

12. DISTRIBUTION/AVAILABILITY STATEMENT
Approved for public release; distribution unlimited

13. SUPPLEMENTARY NOTES

14. ABSTRACT

15. SUBJECT TERMS

16. SECURITY CLASSIFICATION OF:			17. LIMITATION OF ABSTRACT	18. NUMBER OF PAGES	19a. NAME OF RESPONSIBLE PERSON
a. REPORT	b. ABSTRACT	c. THIS PAGE			
unclassified	**unclassified**	**unclassified**	**Same as Report (SAR)**	**14**	

respected here) mean some symbols take on more than one meaning depending on context: subscripts are therefore used, and meanings are defined in the tables.

THE EVALUATION OF EMITTANCE FROM A PLANAR SURFACE

Methodology

The normalized rms emittance for a particle beam propagating in the z direction is defined by[8]

$$\varepsilon_{n,\mathrm{rms}} = \frac{\hbar}{mc}\sqrt{\langle x^2\rangle\langle k_x^2\rangle - \langle xk_x\rangle^2}, \tag{1}$$

where x is position and $\hbar k_x$ is momentum, in keeping with quantum mechanical methods to be used below which rely on conjugate variables. Expectation values are given by $\langle O\rangle \equiv \int O f(\mathbf{r},\mathbf{k}) d\mathbf{r} d\mathbf{k}$, where f is the normalized distribution of the *emitted* electrons: thus, $\langle x^2\rangle$ and $\langle k_x^2\rangle$ are moments of the distribution with analogous equations along the other axes y and z. It is often assumed that $\langle xk_x\rangle^2$ is negligible, but this must be shown, and in the case of a single emitter, it cannot be neglected. Further, $f \propto D(k_z) f_{\mathrm{FD}}[E(\mathbf{k})]$, where the z direction is normal to the surface, $\hbar k_z$ is the momentum into the barrier, D is the transmission probability, and f_{FD} is the Fermi–Dirac distribution, parameters upon which they depend are in Table I (and the notation respects earlier work.[9]) For energy parabolic in momentum, usage of E rather than k in D and f is convenient. Evaluation of the moments is performed in the xy-plane: for thermal and photoemission, that plane is the surface of the cathode, but for field emission, the location of that plane and the distribution on it must be established. First, however, thermal and photoemission emittance are contrasted with field emission emittance in 1D.

Thermal emission

For uniform thermal emission, the emitted distribution is independent of position, and so $\langle x^2\rangle = \rho_c^2/2$. The transmission probability is a step function in energy, making the distribution approximated by the thermal tail, $f \propto \exp(-\beta_T E)$. Current density is proportional to the first moment of the longitudinal velocity $\hbar k_z/m$, and the Richardson–Laue–Dushman equation results. The cross term is zero as it contains integrations over even and odd functions in k_x. The well-known expression for thermal emission results[10,11] and is

$$\varepsilon_{n,\mathrm{rms}}(\mathrm{thermal}) = \frac{\rho_c}{(4\beta_T mc^2)^{1/2}}. \tag{2}$$

Predictions based on Eq. (2) are smaller than measurements. For high power FELs, bunched beams are created by "squeezing" the electron beam from thermionic cathodes producing low current density subject to comparatively low gradient because of space charge and lifetime concerns: the acceleration of the beam is therefore not rapid. The consequences are that emittance increases by a factor of 10–20 over the 1D theory predictions.

Photoemission

Photocathodes switched on and off by short laser pulses generate electron bunches of high brightness and short bunch length.[12–17] Although not as straightforward as for thermionic emission, the emittance of a photocathode has been recently developed. Briefly, the energy implicit in the transmission probability is augmented by the photon energy. Quantum efficiency (such as current density) is proportional to the first moment of the longitudinal velocity and the Fowler–Dubridge relation $QE \propto (\hbar\omega - \phi)^2$ results.[9,18] However, for emittance, the transverse momentum in vacuum $\langle k_\perp^2\rangle$ must also be increased by the photon energy $\hbar\omega$ (Dowell *et al.*[19] have shown that differences in the photoemission emittance between Refs. 11, 20, and 21 are due to the mistaken neglect of photon energy in $k_\perp$ in the former), and it can be shown

$$\varepsilon_{n,\mathrm{rms}}(\mathrm{photo}) \approx \frac{\rho_c}{2}\left(\frac{\hbar\omega - \phi}{3mc^2}\right)^{1/2}. \tag{3}$$

Field emission

In contrast to thermal emission, the transmission probability for field emission is not a step function in energy. Field emission from metals is due to the quantum mechanical tunneling of electrons through a surface barrier from the Fermi level μ. The Fowler–Nordheim transmission probability for the image charge barrier[9,22] is

$$-\ln D_{\mathrm{FN}}(k_z) = \frac{4}{3\hbar F}(2m\Phi^3)^{1/2} v(y) - \frac{2}{\hbar F}(2m\Phi)^{1/2} t(y)(E_z - \mu), \tag{4}$$

where $E_z = (\hbar k_z)^2/2m$ is the "forward" energy. The forms of $v(y)$ and $t(y)$ in Table I are due to Forbes.[23,24] The first moment of the longitudinal velocity $\hbar k_z/m$ results in the Fowler–Nordheim equation. In cylindrical coordinates for which $\langle k_x^2\rangle = \langle k_\perp^2\rangle/2$, using Eq. (4), and invoking the zero-temperature limit of f_{FD},

$$\langle k_\perp^2\rangle = \frac{\int_0^{k_F} dk_z D(k_z) \int_0^{\sqrt{k_F^2 - k_z^2}} k_\rho^2 2\pi k_\rho dk_\rho}{\int_0^{k_F} dk_z D(k_z) \int_0^{\sqrt{k_F^2 - k_\rho^2}} 2\pi k_\rho dk_\rho} \approx \frac{2k_F^2}{\left[\frac{4\mu}{\hbar F}(2m\Phi)^{1/2} t(y) - 1\right]}, \tag{5}$$

where the Fermi momentum k_F and the strong exponential nature of $D(k_z)$ are used. Therefore, the 1D field emission emittance formula is

$$\varepsilon_{n,\mathrm{rms}}(\mathrm{field}) = \rho_c\left(\frac{\hbar k_F}{mc}\right)\left[\frac{4\mu}{\hbar F}(2m\Phi)^{1/2} t(y) - 1\right]^{-1/2}. \tag{6}$$

1D comparisons

Ratios of Eqs. (3) and (6) with the thermal emittance [Eq. (2)] eliminate the cathode radius parameter. The three equations are valid under different conditions, the Fowler–

TABLE I. Terms and values. Definition and values of common terms. "Cu" refers to copper, "Mo" to molybdenum, and "Ba–W" to a barium monolayer on tungsten.

Symbol	Description	Definition/value	Unit
Fundamental constants			
$\hbar$	Planck's constant/2π	0.658 211 89	eV fs
c	Speed of light	299.792 46	nm/fs
m	Electron mass	510 998.9	eV/c^2
α_{fs}	Fine structure constant	1/137.036	
q	Unit charge	$1.602\,176\,5\times10^{-19}$	C
k_B	Boltzmann's constant	1/11604.505	eV/K
ε_0	Permittivity of free space	$8.854\,187\,8\times10^{-11}$	F/m
Distribution function and emission probability			
E	Energy	$\hbar^2k^2/2m$	eV
μ	Chemical potential (Fermi level)	7 [Cu] 5.9 [Mo]	eV
k_F	Fermi momentum term	$\hbar k_F=\sqrt{2m\mu}$	1/nm
Φ	Work function	4.5 [Cu] 2.1 [Ba–W] 4.55 [Mo]	eV
T	Temperature	⋯	K
β_T	Inverse temperature	$1/k_BT$	1/eV
F	Field term	$q\times$electric field	eV/nm
Q	Image charge parameter	$\alpha_{fs}\hbar c/4=0.359\,991\,1$	eV nm
ϕ	Emission barrier above μ	$\Phi-\sqrt{4QF}$	eV
$f_{FD}(E)$	Fermi–Dirac distribution	$\{1+\exp[\beta_T(E-\mu)]\}^{-1}$	
$D(k_z)$	Transmission probability	Ratio of transmitted to incident current density for given k_z	
Thermal, field, and photoemission terms			
A_{RLD}	Richardson constant	120.173 49	$A/K^2\,cm^2$
$J_{RLD}(T)$	Richardson–Laue–Dushman equation	$A_{RLD}T^2\exp(-\phi/k_BT)$	A/cm^2
$v(y)$	Elliptical integral function	$v(y)\approx1-y^2\left(1-\frac{1}{3}\ln(y)\right)$	
$t(y)$	Elliptical integral function	$t(y)\approx1+\frac{1}{2}y^2(1-\ln(y))$	
y	Elliptical integral argument	$y=\sqrt{4QF}/\Phi$	
ρ_c	Cathode radius	⋯	cm
ω	Photon frequency	⋯	rad/s
Field emitter terms			
F_o	Background (asymptotic) field	⋯	eV/nm
β_n	Field enhancement factor	Eq. (36)	
F_{tip}	Apex field	β_nF_o	eV/nm
a_s	Radius of emitter apex	⋯	nm
a_0	Approx. radius of emitter Base; length scale of PCM	⋯	μm
a, a_n	Apex radius factors (dimensionless)	Eqs. (10) and (36)	
β_g	Field enhancement factor due to gate	Eq. (38)	q/nm
N_o	No. of actual emitters on one side of an array quadrant	No. of emitters$=(2N_o+1)^2$	μm
$\Delta(V)$	Fraction of tips emitting	Approximately linear in V	
N	Number of active emitters on one side of an array quadrant	$(2N+1)^2=(2N_o+1)^2\Delta(V)$	
l	Unit cell length scale	Comparable to d_{tt} (Table IV)	μm
L	Array length scale	$L=(2N+1)l$	mm

Nordheim transmission probability is not valid for low field, and field emitters, in particular, are not planar: comparing the 1D emittance formulas for the same parameters is therefore not illuminating. Instead, evaluate $\varepsilon_{n,\mathrm{rms}}$(thermal) for $T=1300$ K, $\varepsilon_{n,\mathrm{rms}}$(photo) for $F=0.1$ eV/nm, and $\varepsilon_{n,\mathrm{rms}}$(field) for $F=7$ eV/nm (all of which are representative values) but otherwise use copper parameters. For a 266 and 213 nm drive laser, ε(photo)/ε(thermal) is then 1.27 and 2.25, respectively, whereas ε(field)/ε(thermal) is 3.31. The ratios reflect that the full width at half maximum of a photo or field emission distribution is larger than the width of the thermal tail of a thermal emission distribution (see, for example,

Fig. 27 of Ref. 25) for metals.

There are caveats. Photoemission and field emission are high brightness sources, capable of in excess of 100 A/cm^2 from small emission areas, and therefore, much smaller active cathode areas are needed. Moreover, improvements in photoemission emittance are more a consequence of superior engineering in forming the beam than advances in physics, e.g., rapidly accelerating the beam from the cathode reduces emittance but requires emission to be bunched or "gated." Therefore, it is somewhat misleading to consider same-sized thermal, photo, and field emission sources or imply that the beams they produce are directly comparable.

THE EVALUATION OF EMITTANCE OF AN ARRAY OF CURVED EMITTERS

Field emission current densities are on the order of 10^8 A/cm^2, but emission sites have nanometer-scale tip radii, and as a result, the active emission area is approximately 50 nm^2. The sharp curvature launches electrons with a transverse momentum component from the start. Placing emitter tips in an array increases the area over which emission occurs. Therefore, the emittance of an array of field emitters is different than Eq. (6): to calculate the emittance, the position and velocity of all electrons crossing an evaluation plane are required (in contrast, for thermal and photoemission, the evaluation plane was the cathode surface).

The expectation values are therefore evaluated in a manner dissimilar from the evaluation of thermal emission, in which current density in the evaluation plane was independent of position. Electron trajectories are followed from the emitter tip to the evaluation plane and are calculated using the point charge model (PCM). By such means, the crossing point will be related to the starting point on the emitter surface. Scaling terms that allow different sized geometries to be compared based on a prolate-spheroidal model (PSM) of an emitter can be found, and we do so, but caution that the PSM is not a substitute for a model such as the PCM to deduce trajectories.

Single ungated emitter in the PSM

Position and velocity in evaluation plane

If inertial effects are ignored (a massless approximation), then field lines overlap trajectory lines. The PSM[26–28] provides field lines analytically. Dimensionless coordinate systems as in Table II make connections with the PCM transparent, allowing for the usage of scaling arguments, and are therefore used. To relate to physical systems, "dimensionless" coordinates can be expressed in the "units" of Table III, although dimensioned terms shall be explicitly given when needed.

The prolate spheroidal (alternately, "ellipsoidal") coordinate system is related to the cylindrical coordinate system (ρ,z) by

$$\rho = \sinh\alpha \sin\beta,$$

TABLE II. Coordinate systems and relationships. Relationships between cylindrical (specifies trajectories), prolate spheroidal (specifies emitter surface) and spherical (specifies spherical emitter apex) coordinates.

Symbol	Description	Definition/relation
ρ, z	Cylindrical coordinates	⋯
α, β	Prolate-spheroidal coordinates	$\rho=\sinh\alpha\sin\beta$ $z=\cosh\alpha\cos\beta$
(ρ_s,z_s) (α_s,β_s)	Emitter surface	α_s is constant
(ρ_h,z_h) (α_h,β_h)	Evaluation plane	z_h is constant
z_h	Height of evaluation plane	$\cosh\alpha_h(\beta)=z_h/\cos\beta$
z_o	Height of emitter	$z_s(0)$
R	Ratio of semimajor to semiminor axes for ellipsoid representing emitter	$\coth\alpha_s$
η	Ratio of evaluation plane to emitter height	z_h/z_o
α, θ	Radius and polar angle of equivalent sphere representing ellipsoid apex for $\rho_s<a$	$\rho_s\approx a\sin\theta$ $z_s\approx z_o-a(1-\cos\theta)$ $\approx z_o-\rho_s^2/2$

$$z = \cosh\alpha\cos\beta, \tag{7}$$

where α and β are the angular coordinates, and because ρ and z are dimensionless, the usual dimensioned coefficient on the right hand side is omitted. The emitter surface is defined by a constant $\alpha=\alpha_s$, where the s subscript designates "surface." Field lines are defined by constant β. The evaluation plane is defined by $z=z_h$. The relationship between prolate spheroidal surface and evaluation plane coordinates (along side a polar coordinate (a,θ) equivalent sphere surface) is shown in Fig. 1. Also shown is the field line (red or curved) compared to a massive particle trajectory (blue or straight).

The field lines originate on the surface at (ρ_s,z_s) and cross the evaluation plane at (ρ_h,z_h). Therefore, the relationship between ρ_s and ρ_h is

$$\rho_h = \frac{\sinh\alpha_h}{\sinh\alpha_s}\rho_s, \tag{8}$$

where, because z_h is constant, α_h is a function of β and therefore ρ_s, and because α_s is a constant, z_s is a function of β only. If the ratio of the semimajor to the semiminor axis of the ellipsoid is R, and the ratio of height of the evaluation plane to height of the emitter is $\eta=z_h/z_s(0)\equiv z_h/z_o$, then very close to the emitter apex where emission is dominant, using notation summarized in Table II, we find

TABLE III. Dimensionless units conversion factors. "Dimensionless" parameters are understood to be in the following units based on the choice of length and energy scales. The "Representative value" column expresses quantities in SI units if $a_0=1$ μm and $F_o=10q$ MV/m.

Term	Definition/relation	Representative value
Length	a_0	1 μm
Energy	$F_o a_0$	10 eV
Mass	m	5 110 998.9 eV/c^2
Velocity	$(2F_o a_0/m)^{1/2}$	1 875 537 m/s
Time	$(ma_0/2F_o)^{1/2}$	0.533 180 5 ps
Wave number	$k_0\equiv(2mF_o a_0)^{1/2}/\hbar$	16.200 88 nm^{-1}

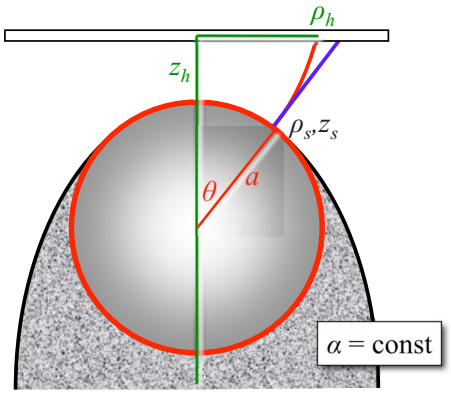

FIG. 1. (Color online) Geometry of an ellipsoidal field emitter, showing cylindrical coordinates along the emitter surface (ρ_s, z_s) and along the evaluation plane (ρ_h, z_h). The equivalent sphere characterized by (a, θ) is also shown. The red (curved) line from the surface indicates a field line, whereas the blue (straight) line shows the trajectory of a massive particle emitted with an initial velocity.

$$\rho_h \approx \rho_s \sqrt{(z_h^2 - 1)(R^2 - 1)}. \tag{9}$$

When inertial effects are included, ρ_h/ρ_s will differ from Eq. (9). From Eq. (8) and the definition of apex radius,

$$a = [-\partial_\rho^2 z|_{\rho=0}]^{-1} = \frac{\cosh(\alpha_s)}{\sinh^2(\alpha_s)},$$

$$R(a) = \left\{ \frac{1}{2a}[a + (4 + a^2)^{1/2}] \right\}^{1/2}. \tag{10}$$

The R^2 term in the radical of Eq. (9) dominates for Spindt-type emitters so that $R^2 - 1$ goes as $1/a$ when $a \ll 1$.

The initial velocity v_e is approximated by the relationship between the current density J_e and the number density ρ_e using $J_e = q\rho_e v_e$ and is directed normal to the emitting surface. To leading order, the magnitude of the velocity is

$$v_e = \frac{J_e}{q\rho_e} = \frac{\int \frac{\hbar k_z}{m} D(k_z) f_{\mathrm{FD}}(\mathbf{k}) d\mathbf{k}}{\int D(k_z) f_{\mathrm{FD}}(\mathbf{k}) d\mathbf{k}} \approx \frac{\hbar k_F}{m} \tag{11}$$

as a consequence of the strongly peaked nature of the integrand in k_z. The final velocity magnitude is obtained from the initial velocity and the potential difference between the location on the evaluation plane and the emitter surface.

Distribution of electrons in the evaluation plane

The symmetry of the unit cell emitter implies that the distribution of electrons will depend only on the cylindrical coordinate ρ and not on the angle φ. Denote the distribution of electrons in the evaluation plane by $P(\rho_h)$. For a single emitter, $x = a_0 \rho \cos\varphi$ and so

$$\langle x^2 \rangle = a_0^2 \left(\frac{\int_0^{2\pi} d\varphi \int_0^\infty (\rho \cos\varphi)^2 P(\rho) \rho d\rho}{\int_0^{2\pi} d\varphi \int_0^\infty P(\rho) \rho d\rho} \right) = \frac{1}{2} a_0^2 \langle \rho^2 \rangle, \tag{12}$$

and similarly with $k_x = k_0 k_\rho \cos\varphi$ it follows

$$\langle k_x^2 \rangle = \tfrac{1}{2} k_0^2 \langle k_\rho^2 \rangle,$$

$$\langle x k_x \rangle = \tfrac{1}{2} a_0 k_0 \langle \rho k_\rho \rangle, \tag{13}$$

where the a_0 and k_0 terms of Table III handle units, the h subscript on ρ is suppressed, and evaluation in the z_h plane is understood. Therefore,

$$\varepsilon_{n,\mathrm{rms}}|_{\text{single emitter}} = \frac{\hbar}{4mc} a_0 k_0 (\langle \rho^2 \rangle \langle k_\rho^2 \rangle - \langle \rho k_\rho \rangle^2)^{1/2}. \tag{14}$$

The function $P(\rho_h)$ is a ratio of current density at ρ_h to current density on axis. Therefore, there are two considerations to P: the magnitude of the current density at the emitter surface and how it declines through beam expansion at the evaluation plane. At the surface, the emission current J_e is related to the field $F(\rho_s)$ via the Fowler–Nordheim equation: we use the Murphy and Good (MG) form[9,22] with the Forbes approximation to $v(y)$ and $t(y)$:[23,24] the log terms in $v(y)$ changes the MG form to

$$J_e(F) = AF^{2-\kappa} \exp(-B/F), \tag{15}$$

where A, B, and κ are given by

$$\kappa = \frac{8Q}{9h} \sqrt{\frac{2m}{\Phi}},$$

$$A = \frac{q}{16\pi^2 \hbar \Phi t(y_o)^2} \left(\frac{\Phi^2 e^6}{4Q} \right)^\kappa,$$

$$B = \frac{4}{3\hbar} \sqrt{2m\Phi^3}, \tag{16}$$

and where B is equivalent to B_{FN} in Eq. (40) of Ref. 9, $y_o = e^{-1/2} = 0.6065$, and $t(y_o) = 1 + (1/6e) = 1.061$ [y_o optimizes a quadratic fit to $v(y)$ for metals[29]]. For copper, $\kappa = 0.772\,81$, $B = 65.207$ eV/nm, and $A = 62.182$ A/cm^2(cm/eV)$^{2-\kappa}$.

The current density J_h in the z_h plane is related to the current density on the surface by conservation of particle number, for which

$$\Delta Q = 2\pi\rho_s \sqrt{1 + \left(\frac{\partial z_s}{\partial \rho_s} \right)^2} J_e[F(\rho_s)] \Delta\rho_s = 2\pi\rho_h J_h(\rho_h) \Delta\rho_h, \tag{17}$$

where ΔQ is the emitted charge in unit time in a ribbon of width $\Delta\rho_s$ on the surface and $\Delta\rho_h$ in the z_h plane. Close to the emitter apex, the surface is given by $z_s(\rho_s) \approx z_o - \rho_s^2/2a$ so that $\partial z_s/\partial\rho_s \approx -\rho_s/a$. Solving for J_h then identifies $P(\rho_h)$ in Eq. (12) as

$$P(\rho_h) = \frac{J_h(\rho_h)}{J_h(0)} = \sqrt{1 + \left(\frac{\rho_s}{a} \right)^2} \left\{ \frac{J_e[F(\rho_s)]}{J_e(F_{\mathrm{tip}})} \right\}. \tag{18}$$

The field at the apex is $F(\rho_s = 0) \equiv F_{\mathrm{tip}}$. Along the spherical apex, F falls as $F_{\mathrm{tip}} \cos\theta$ [Table III and the discussion following Eq. (36) below] so that

$$\frac{J_e[F(\rho_s)]}{J_e(F_{\text{tip}})} = \exp\left\{-\frac{B}{F_{\text{tip}}}\left[\frac{1}{\cos\theta(\rho_s)} - 1\right]\right\} = \exp\left[-\frac{B}{2F_{\text{tip}}a^2}\rho_s^2\right]. \tag{19}$$

Therefore, $P(\rho_h)$ in Eq. (12) is approximated by a Gaussian in the evaluation plane, or

$$P(\rho_h) \approx \exp(-C\rho_h^2),$$

$$C \sim C_{\text{PSM}} = \frac{B}{2F_{\text{tip}}a^2[(\eta^2-1)R^2+1]} \approx \frac{B}{2F_{\text{tip}}a(\eta^2-1)}, \tag{20}$$

where the tilde indicates that although C is similar C_{PSM}, the latter is only approximate and so C is to be numerically found from the PCM.

In the evaluation plane, the radial velocity changes with distance from the axis. A good approximation is

$$k_\rho(\rho_h) \approx \gamma_1\rho_h - \gamma_3\rho_h^3. \tag{21}$$

The γ coefficients are determined numerically, although a crude approximation for γ_1 alone may be made by assuming motion in a constant field near the axis, or

$$\gamma_1 \sim \frac{1}{z_h - z_o}\left[\frac{(z_h - z_o)F_{\text{tip}}a_0 + \mu}{F_o a_0}\right]^{1/2} \approx \left[\frac{F_{\text{tip}}}{F_o z_o(\eta-1)}\right]^{1/2}, \tag{22}$$

where, as with Eq. (20), the right hand side is only approximate. Using Eq. (21) it is found

$$\langle\rho^2\rangle\langle k_\rho^2\rangle = \langle\rho^2\rangle[\gamma_1^2\langle\rho^2\rangle + 2\gamma_1\gamma_3\langle\rho^4\rangle + \gamma_3^2\langle\rho^6\rangle],$$

$$\langle\rho k_\rho\rangle^2 = \gamma_1^2\langle\rho^2\rangle^2 + 2\gamma_1\gamma_3\langle\rho^2\rangle\langle\rho^4\rangle + \gamma_3^2\langle\rho^4\rangle^2. \tag{23}$$

Making use of the relation

$$\int_0^\infty \rho^{2n}P(\rho)\rho d\rho = \int_0^\infty \rho^{2n}e^{-C\rho^2}\rho d\rho = \frac{\Gamma(n+1)}{2C^n}, \tag{24}$$

where $\Gamma(n)$ is the gamma function, the emittance for a single emitter is then found to be

$$\varepsilon_{n,\text{rms}}|_{\text{single emitter}} = \frac{\hbar}{\sqrt{2}mc}a_0k_0\left(\frac{\gamma_3}{C^2}\right), \tag{25}$$

where the γ_1 terms cancel. Using a generic $\gamma_3=27$ and $a_0k_0=8\times10^4$ from the trajectory analysis (below), and C_{PSM} indicates that $\varepsilon_{n,\text{rms}}\sim360\hbar/mc$. Therefore, single emitters are exceptionally low emittance and high brightness sources. For arrays of emitters, the γ_1 terms do not cancel, the cross term is negligible if the number of emitters is large, and the array emittance is much larger.

It must be emphasized that the PSM is only an approximation for the shape of a Spindt-type emitter and, more importantly, because it neglects electron inertial effects, it is increasingly inaccurate in estimating ρ_h and $k_\rho(\rho_h)$ as the evaluation plane is further removed from the apex: if $\eta\gg1$ then PSM predicts that $k_\rho(\rho_h)$ is vanishing, which is incorrect. However, the *parametric* dependence on geometry and field is good, so extrapolating to other conditions or configurations from a numerical baseline example is possible.

Multiple ungated emitters

Periodicity of an array

Assume all field emitters of an array are geometrically identical and operate under the same conditions—the approximations are not strictly true because emitters vary among themselves[30] and those at the boundary of the emission area will experience a higher field. Cartesian coordinates are required for a rectangular array. The Gaussian nature of $P(\rho_h)$ allows for a simplification in the evaluation of quantities in one Cartesian dimension x, such that the mean value of a function $O(x)$ is

$$\langle O(x)\rangle = \frac{\int O(x)f(x,k_x)dxdk_x}{\int f(x,k_x)dxdk_x}, \tag{26}$$

where $f(x,k)$ is constructed from $P(\rho)$ for the spatial distribution of emitters, but for which an explicit form is unnecessary. All that is important is that for an array, f will be periodic: if the unit cell has dimensions l, then $f(x+jl)=f(x)$ for integer j. If the length of the side of an array is L then

$$\int_{-L/2}^{L/2} f(x)dx = \sum_{j=-N}^{N}\int_{-l/2}^{l/2} f(x+jl)dx = (2N+1)\int_{-l/2}^{l/2} f(x)dx, \tag{27}$$

where $(2N+1)l=L$ and $(2N+1)^2$ is the number of emitters in a square. Thus,

$$\int_{-L/2}^{L/2} x^2f(x)dx = \sum_{j=-N}^{N}\int_{-l/2}^{l/2}(x+jl)^2f(x+jl)dx = (2N+1)\int_{-l/2}^{l/2}x^2f(x)dx + \left(\sum_{j=-N}^{N}j^2\right)l^2\int_{-l/2}^{l/2}f(x)dx. \tag{28}$$

The summation on the second line is analytic. Therefore,

$$\langle x^2\rangle = \tfrac{1}{3}N(N+1)l^2 + \langle x^2\rangle_o,$$

$$\langle x^2\rangle_o = \frac{\int_{-l/2}^{l/2}x^2f(x)dx}{\int_{-l/2}^{l/2}f(x)dx}, \tag{29}$$

where the second line refers to the unit cell or single emitter and is so indicated by the o subscript. For field emitters, f vanishes at the boundaries $l/2$, but the thermal result is recovered if $f=1$ (uniform emission), for which Eq. (29) becomes $\langle x^2\rangle=[4N(N+1)+1]l^2/3=L^2/12$. For arrays, the N terms dominate the unit cell term. Similarly, k_x will exhibit the same periodicity as f, and so

$$\int_{-L/2}^{L/2} O(x)f(x)dx = \sum_{j=-N}^{N} \int_{-l/2}^{l/2} O(x+jl)f(x+jl)dx$$
$$= (2N+1)\int_{-l/2}^{l/2} O(x)f(x)dx. \quad (30)$$

Therefore, $\langle k_x^2\rangle_o = k_o^2\langle k_\rho^2\rangle_o$ as long as $P(l/2)$ is negligible. An analogous derivation shows that $\langle xk_x\rangle = \langle xk_x\rangle_o$.

Array emittance

Ignoring boundary terms reflects that the array is infinite. A systematic study by Rhee *et al.*[31] for finite sized arrays obtains a similar expression to ours in their case 1 (parallel beam) example: their geometric factor G_R is equivalent to $(l^2/3)(1+N^{-1})(N+1/2)^2$ and is a factor of $1+(1/N)$ larger than ours. For N sufficiently large, as with usual arrays, the difference is negligible. A finite sized array experiences space charge forces that cause emission from the edge of the array to bend away from the center. This is analogous to the focal length parameter of Rhee being finite. An infinite focal length limit, as presumed by the periodicity assumption, means that the beamlets are parallel: if they were not, additional terms of order $1/(2N+1)$ and $1/(2N+1)^2$ arise. Using $\langle x^2\rangle \approx N(N+1)l^2/3$ and $\langle xk_x\rangle = k_0a_0\langle \rho k_\rho\rangle/2$, the emittance for an array is

$$\varepsilon_{n,\mathrm{rms}}|_{\mathrm{array}} = \frac{\hbar}{mc}\sqrt{\frac{N(N+1)}{6}(k_0l)^2\langle k_\rho^2\rangle_o - \frac{1}{4}(k_0a_0)^2\langle \rho k_\rho\rangle_o^2}. \quad (31)$$

Observe that $\langle \rho k_\rho\rangle_o^2 = (\gamma_1/C)^2$ is small compared to $\langle k_\rho^2\rangle_o = \gamma_1^2/C$, so that the cross term is negligible, and so to leading order,

$$\varepsilon_{n,\mathrm{rms}}|_{\mathrm{array}} \approx \gamma_1\frac{\hbar}{mc}(k_0l)\left[\frac{N(N+1)}{6C}\right]^{1/2}. \quad (32)$$

Using Eq. (32) requires attention to three subtleties: first, γ_1 and C are evaluated numerically although PSM can give order of magnitude estimates; second, l is a length scale characteristic of the unit cell of a single emitter, but is not identical to the tip-to-tip separation *unless* all emitters are active; third, $(2N+1)^2$ is the number of *active* emitters.

The PCM and trajectory parameters

Mono- and dipole potentials

The PCM, introduced in a previous study,[29] analytically gives field enhancement and tip radii parameters. A line of charges is placed such that the resulting zero equipotential line approximates the shape of an emitting structure. Previously, the PCM stacked charges of one sign above the $z=0$ plane to approximate the shape of the emitter created by melting and field formation. The potential then is given by

$$V(\tilde{\rho},\tilde{z}) \equiv F_o a_0 V_n\left(\frac{\tilde{\rho}}{a_0},\frac{\tilde{z}}{a_0}\right),$$

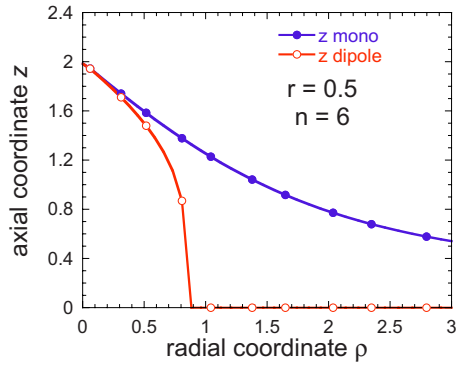

FIG. 2. (Color online) Comparison of mono (blue or cusplike) and dipole (red or ellipsoidal-like) surfaces in the PCM for the parameters $r=0.5$ and $n=6$.

$$V_n(\rho,z) \equiv -z + (\rho^2+z^2)^{-1/2} + \sum_{j=1}^{n}\frac{\lambda_j}{[\rho^2+(z-z_j)^2]^{1/2}}, \quad (33)$$

where a_0 is a (dimensioned) characteristic length of the base and $(\tilde{\rho},\tilde{z})$ are the laboratory coordinates. The λ_j are determined by the boundary condition $V_n(0,z_{n+1})\equiv 0$, which results in a matrix equation that can be inverted to recover the λ_j's. Importantly, ρ and z, and likewise V_n, are dimensionless, allowing for scaling arguments to be made. The point charge locations are defined by

$$z_n = \sum_{j=1}^{n-1} r^{n-1} = \frac{1-r^n}{1-r}, \quad (34)$$

where r is a scaling parameter governing the magnitude of a point charge compared to the one below it. As charges of only one sign are used, V_n in Eq. (33) is termed the "monopole" model $V_n^{\mathrm{mono}}(\rho,z)$. Observe that the first charge has been explicitly pulled out of the summation (i.e., $\lambda_0=1$ and z_j for $j=0$ is zero).

Spindt-type field emitters by comparison are sharper and more conical. Therefore, introduce a "dipole" potential V_n^{dipl} defined by (no charge at $z=0$ means $\lambda_0=0$)

$$V_n^{\mathrm{dipl}}(\rho,z) \equiv -z + \sum_{j=1}^{n}\lambda_j\{[\rho^2+(z-z_j)^2]^{-1/2} - [\rho^2+(z+z_j)^2]^{-1/2}\}, \quad (35)$$

which also satisfies $V_n^{\mathrm{dipl}}(0,z_{n+1})=0$, but which produces a sharper emitter as shown in Fig. 2 for $r=0.5$ and $n=6$.

The trajectories are found by launching electrons with a velocity $\hbar k_F/m$ normal to the surface defined by $V_n(\rho_s,z_s)\equiv 0$. The equations of motion are numerically integrated until the electrons cross the z_h plane, at which point the value of ρ_h is found. From the relationship between ρ_h and $k_\rho(\rho_h)$, the numerical values of the γ's are obtained. The value of C is obtained from the behavior of the current density distribution in the h plane.

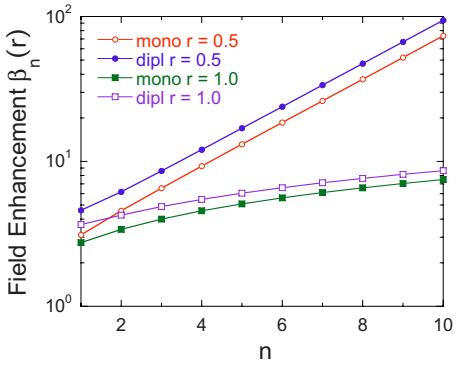

FIG. 3. (Color online) Field enhancement factors as a function of n for the mono and dipole emitter types for values of $r=0.5$ and 1.0. For large n, the dipole field is approximately 30% larger, even though the apex radii are nearly the same, for $r=0.5$.

Field enhancement, apex radii factors, and field drop-off

The field enhancement factor is defined as the ratio of the apex field F_{tip} to F_o, whereas the apex radius is a ratio of the first and second derivatives of V_n on axis, or

$$\beta_n(r) = -\left.\partial_z V_n(0,z)\right|_{z=z_{n+1}},$$

$$a_n(r) = -\left.\frac{\partial_\rho V_n(\rho,z)}{\partial_\rho^2 V_n(\rho,z)}\right|_{\substack{\rho=0\\ z=z_{n+1}}}, \tag{36}$$

and they are dimensionless. From Eqs. (33) and (35), the evaluations are straightforward but lengthy. A comparison of β_n for $r=0.5$ and 1.0 for the monopole and dipole geometries is shown in Fig. 3 and the same for a_n in Fig. 4. Likewise, the quality of the approximation $F(\rho)=F_{\text{tip}}\cos\theta(\rho)$, where $\rho=a\sin\theta$, is shown in Fig. 5, where the line marked "Numerical" is calculated using the PCM. The evaluation plane z_h is chosen such that trajectories from adjacent emitters are not present in the unit cell, and therefore, z_h-z_o is larger than several tip radii but smaller than 1.

Relation to physical Spindt-type emitters

Emitter geometry specification

The emitters characterized by Schwoebel *et al.*[32] and summarized in Table IV will be taken as the base-line geometry. The apex field F_{tip} will be inferred from *I-V* data. A

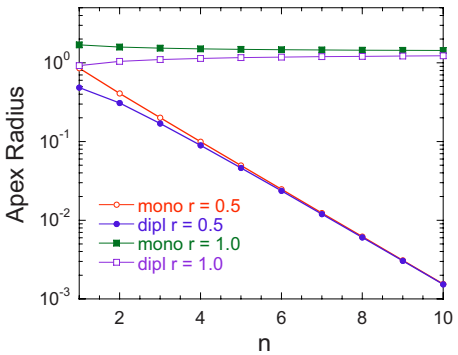

FIG. 4. (Color online) Same as Fig. 3, but for the apex radius: for large n, the estimates converge.

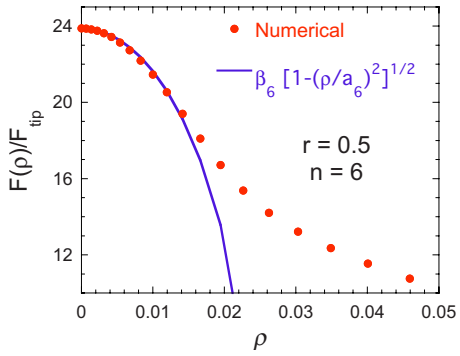

FIG. 5. (Color online) Variation of field along the surface of a dipole geometry as a function of axial coordinate ρ, showing the nature of the field drop off compared to its apex value and the quality of the approximation $F=F_{\text{tip}}\cos\theta$ used to derive C_{PSM}.

model for the "notional" emission area[33] [the ratio of total current I_{tip} to current density on axis $J_e(F_{\text{tip}})$] was developed separately[34] but its leading order behavior shall be used here. We have

$$I_{\text{tip}}(V_g) = 2\pi a^2 g(F_{\text{tip}}) J_e(F_{\text{tip}}),$$

$$g(F) = \frac{0.8F}{[B+(1-\kappa)F]}. \tag{37}$$

The on-axis field F_{tip} is obtained from the gate potential V_g by $F_{\text{tip}}=\beta_g V_g$, where the approximation developed in Ref. 35 is used and is (for terms defined in Table IV)

$$\beta_g(a_s) = \frac{q}{a_s}\left\{\frac{\pi}{\ln\left[\frac{a_g}{54a_s}\cot\beta_c\left(86+\frac{a_g}{a_s}\right)\right]} - \tan^2\beta_c\right\}. \tag{38}$$

The apex radius a_s is adjusted until a theoretical current of 0.5 μA occurs for the same voltage as experimentally reported. This *one data point* determination is not a fit over many data points: therefore, the degree to which Eq. (37)

TABLE IV. Baseline FEA unit cell parameters. Parameters based on the F1 emitter shown in Figure 1 (I–V characteristics of which are shown in Figure 2) of Ref. 32. A_{FN} and B_{FN} refer to the least-squares straight line fits to $\ln(I_{\text{FN}}/V^2)\approx\ln(A_{\text{FN}})-B_{\text{FN}}/V$ (the conventional representation).

Symbol	Meaning	Value	Unit
a_s	Tip apex radius	12.4	nm
a_g	Gate radius	0.375	μm
β_c	Emitter cone angle	17	deg
d_{tt}	Tip-to-tip separation	1.5	μm
d_{bg}	Base-to-gate separation	1.2	μm
t_b	Base layer thickness	0.18	μm
t_g	Gate layer thickness	0.75	μm
Φ	Work function	4.55	eV
K_s	Oxide dielectric constant	3.75	
σ	Metal conductivity	18	$1/(\Omega\,\mu\text{m})$
λ	Saturn mode correction factor	1.2	
w	Square array width	0.1	cm
A_{FN}	Exp. FN I(V) parameter	8.09	$\mu\text{A}/\text{cm}^2\,\text{V}^2$
B_{FN}	Exp. FN I(V) parameter	1.72	kV
ω	Gate sinusoidal frequency	$2\pi/\delta$	1/ps
δ	Rise time	1–50	ps

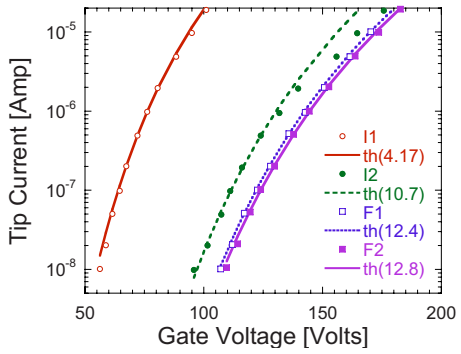

FIG. 6. (Color online) Comparison of analytical tip current model to the experimental data of Schwoebel *et al.* (Ref. 32) for a single tip, in which conditioning was shown to bring different emitters to a comparable performance, interpreted as a change in apex radius. Labels are those of Schwoebel *et al.*; lines are theory calculated using Eq. (37).

reproduces experimental curves is an indication of its utility. The tip radii a_s found for the curves labeled I1, I2, F1, and F2 of Fig. 2 of Ref. 32 are 4.17, 10.7, 12.4, and 12.8 nm, respectively. The predicted current-voltage theory and the data of Schwoebel *et al.* are shown in Fig. 6. The agreement indicates that Eq. (37) successfully determines the permissible tip radii: we choose one corresponding to a "conditioned" emitter.

Prediction of emittance for a Spindt-type array

A molybdenum ungated field emitter dipole PCM with $r=0.5$, $n=7$, and a base radius of $a_0=1$ μm gives the apex radius as $a_s=a_7a_0=12.0$ nm. A background field of 241 MV/m (the field *within* the unit cell and therefore higher than the anode-cathode field) of a gated FEA is reasonable,[26] corresponds to $F_o=0.241$ eV/nm, and gives $F_{\rm tip}=8.11$ eV/nm, $J_e(F_{\rm tip})=8.48\times10^7$ A/cm^2, and $k_0=79.5$ nm^{-1}. An evaluation plane at $z_h=2.5$ entails that $\eta=1.255$. A numerical evaluation of the trajectories and an extraction of γ and C from $k_\rho(\rho_h)$ and $P(\rho_h)$ plots, respectively, gives $\gamma_1=12.7$, $\gamma_3=26.8$, and $C=81.4$ (compare to estimates based on PSM, which give $\gamma_1=8.15$ and $C_{\rm PSM}=65.3$, respectively: although of the right magnitude they would predict an emittance 60% of its numerical value).

Actual emitter radii in an array follow a log-normal distribution,[36,37] making the estimation of the number of emitters operating for a given gate voltage rather involved. An estimate of number of tips emitting is reasonably well characterized by a function Δ linearly dependent on gate voltage. Spindt-type emitters[38] have shown current densities comparable to 2000 A/cm^2. Therefore, the current from an array is taken to be

$$I_{\rm array}(V_g)=2\pi a_s^2 g(\beta_g V_g)(2N_o+1)^2\Delta(V_g)J_e(\beta_g V_g). \quad (39)$$

The number of active emitters is $(2N+1)^2\Delta(V_g)$ if $(2N_o+1)^2$ is number of emitters in the array. It shall be assumed that 40% of the emitters are active at a gate voltage of 136 V: therefore, a gate voltage of 200 V is required to produce a current density of 2000 A/cm^2 from a square array $L=0.2$ cm on a side if the tip-to-tip spacing is 1.5 μm. The unit cell length l is determined from $L/l=(2N_o+1)\sqrt{\Delta(V_g)}$, and so the emittance in the limit of large N_o is

$$\varepsilon_{n,\rm rms}|_{\rm array}=\gamma_1\frac{\hbar}{mc}\frac{k_0L}{\sqrt{24C\Delta(V_g)}}. \quad (40)$$

It is therefore predicted that for a current density of 2000 A/cm^2 from a square array of 0.2 cm on a side, the emittance is 23 mm mrad.

Comparison to experimental emittance measurements

Comparing the theoretical emittance formula to experimental data is hampered by the scarcity of experimental data of beams generated from field emitters (more often, beams from photofield emission from arrays[39,40] and single tips and needles[41–47] are reported). Two topical cases are Jarvis *et al.*[48] and Leeman.[49] Modifications and complications to the theory are discussed for each.

Jarvis *et al.* considered diamond pyramidal field emitters and find $\varepsilon_{n,\rm rms}({\rm Jarvis})\approx0.97$ mm mrad. Diamond and metal emitters are categorically different, but semiconductor emitters do have performance characteristics similar to metal ones even though the underlying physics of emission differs:[50] therefore, as a first approximation, only those parameters that depend on layout and measurement conditions will be altered from the previous analysis. Converting the layout of Jarvis *et al.* of a tip-to-tip (pitch) separation of 28 μm and the array in the form of a 3×24 rectangle into an equivalent square, L becomes 0.0238 cm. A maximum extraction field of $F_o=17$ eV/μm was reported. Lastly, the emitters were conditioned such that Δ was suggested to be near unity. Therefore, theory predicts

$$\varepsilon_{n,\rm rms}\,({\rm Jarvis})|_{\rm theory}=\gamma_1\frac{\hbar}{mc}L\sqrt{\frac{F_oma_0}{12C}}\approx0.88\ {\rm mm\ mrad}, \quad (41)$$

where the base radius of the diamond emitters was taken to be $a_0=2.5$ μm. As N is not large ($N=4$ corresponds to a square array of 81 emitters, slightly larger than the 72 of Jarvis *et al.*), the $1+(1/N)$ factor of Rhee for finite arrays suggests the theory value be raised to 1.1 mm mrad.

Leeman *et al.* considered 50 000 gated metal emitters ($N_o=111$) emitted from a disk of 0.1 cm in diameter ($L=0.0886$ cm) and reported an emittance of 2.5 mm mrad. Emitters that have not been extensively conditioned show a significantly smaller Δ compared to those that have,[51] so that on the order of 5% of the emitters operating is expected. The *I-V* data of Leeman *et al.* in their Fig. 2 is well modeled by retaining most of the Spindt-like parameters but changing $n=6$ in the PCM, to give $a_s=22$ nm and $F_o=0.215$ eV/nm. A comparison of Leeman's Fig. 2 data with theory is shown in Fig. 7. The trajectory simulations then give $\gamma_1=12.1$, $\gamma_3=21.4$, and $C=88.2$. An array current of 1.67 mA at a voltage of 195 V corresponds to $\Delta(195\ {\rm V})=0.0412$ and $N=23$. Therefore, we shall project to an array delivering 1 A/cm^2 from an area of 0.7854 mm^2 at a voltage of 205 V. The smallness of Δ creates an interpretation problem: the active emitters can be uniformly distributed over the array or, as is more likely, a hot spot of active emitters can occur. The later

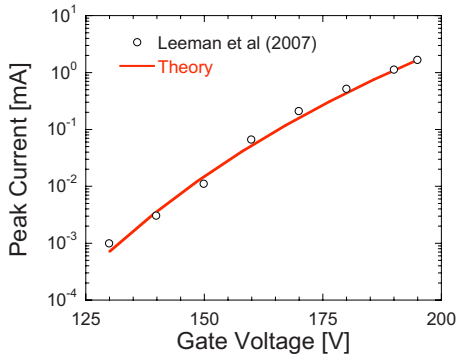

FIG. 7. (Color online) Comparison of analytical array current model to the experimental data of Leeman *et al.* for an array in which on the order of 5% of the emitters are active.

case shall be modeled by assuming all the active emitters are adjacent in a smaller square area. In the "uniform" case, $l = 19\ \mu\text{m} = 4.8 d_{tt}$, and

$$\varepsilon_{n,\text{rms}}\ (\text{Leeman})|_{\text{spread out}} = \gamma_1 \frac{\hbar}{mc} L \sqrt{\frac{F_o m a_0}{12C}} \approx 6.76\ \text{mm mrad}. \quad (42)$$

Conversely, in the "hot spot" case, $l = d_{tt}$ and

$$\varepsilon_{n,\text{rms}}\ (\text{Leeman})|_{\text{packed}} = \gamma_1 \frac{\hbar}{mc} d_n (2N+1) \sqrt{\frac{F_o m a_0}{12C}} \approx 1.41\ \text{mm mrad}. \quad (43)$$

The measurement reported by Leeman *et al.* falls between these limits and suggests that the array is closer to the hot spot configuration than a uniformly distributed one.

3D comparisons

Cathodes are operated under different conditions to accommodate their limitations. The beam drawn from the cathode experiences different acceleration gradients depending on the gun: for example, dc photoinjector has a smaller gradient at the photocathode than does a rf photoinjector. Constraints on the bunches themselves likewise depend on the technology. Therefore, comparing the emittances of the thermal, photo, and field emission cathodes directly for same cathode dimensions and operating conditions would be misleading. Rather, conditions reflecting the operational environment typical of each cathode at a performance level relevant to that cathode will be considered. Note that emittance is not the only metric. The amount of charge in an electron bunch is important for accelerators and relates to current and pulse duration. Brightness goes as the ratio of current to emittance squared ($B_{n,\text{rms}} \propto I/\varepsilon_{n,\text{rms}}^2$), with high brightness being desirable. In general, thermionic cathodes are limited by the source temperature (to avoid lifetime issues), photocathodes are limited by extraction field (to avoid space charge issues), and field emitters are limited by maximum gate voltages (to avoid breakdown) or emission areas (to enable fast switching times). Comparisons therefore involve parameters which are quite different. Therefore, a baseline of 1 A is considered, followed by performance values that are more indicative of how the cathodes are intended to be used.

Thermionic cathodes

A circular dispenser cathode of radius $\rho_c = 0.5642$ cm (area = 1 cm^2) with $\Phi = 2.0$ eV subject to a background field of 1 MV/m and at a temperature of $T = 1200$ K produces a current of $I_o = 1$ A with $\varepsilon_{n,\text{rms}} = 1.269$ mm mrad. Larger total currents are enabled by higher temperatures or larger cathode diameters, and greater charge in the bunch is obtained by longer pulse durations and later compression of the beam. If the temperature is $T(x) = (1+x)1200$ K, then

$$I(x) = (1+x)^2 \exp\left(8.97 \frac{x}{1+x}\right) I_o,$$

$$\varepsilon_{n,\text{rms}}(x) = \sqrt{1+x}\,\varepsilon_{n,\text{rms}}(0). \quad (44)$$

Thus, to obtain 100 A of current, the cathode radius can be increased to 5.64 cm or the temperature increased to 1533 K (i.e., $x = 0.277$), causing the emittance to become 12.7 or 1.434 mm mrad, respectively. Thermionic cathodes cannot be modulated rapidly enough to produce pulse lengths of 10–50 ps.

Photocathode

A copper photocathode subject to a background field of 50 MV/m, and illuminated with a 255 nm laser of intensity of 10^4 W/cm^2 over a circular area with radius of 0.794 cm exhibits a theoretical quantum efficiency[20] of 0.0246% and produces a current of $I_o = 1$ A with $\varepsilon_{n,\text{rms}} = 1.93$ mm mrad. If $\rho_c(x) = 0.794(1+x)$ cm, then

$$I(x) = (1+x)^2 I_o,$$

$$\varepsilon_{n,\text{rms}}(x) = (1+x)\varepsilon_{n,\text{rms}}(0). \quad (45)$$

Modifying fields and intensities to match the Linac Coherent Light Source values reported by Schmerge *et al.*,[52] in which a 1 nC charge bunch is generated by a 255 nm laser of radius of 1.2 mm for approximately 10 ps subject to a background field of 120 MV/m, the current and current density are then 100 A and 2210 A/cm^2, respectively, and the theoretical emittance is 0.427 mm mrad. Photocathodes can easily produce pulse lengths of 10–50 ps.

Field emitter array

For molybdenum Spindt-type emitters with the number of emitters given by $2N+1 = \pi\rho_c^2/d_{tt}^2 = 667$ (i.e., $\rho_c = 564\ \mu$m) with apex radii of 12 nm and Table IV parameters otherwise, subject to a gate voltage of 161.3 V, then the array current density with 40% emitting is 100 A/cm^2, and the current is $I_o = 1$ A with $\varepsilon_{n,\text{rms}} = 7.31$ mm mrad. If $V(x) = 161.3(1+x)$ V, then

$$I(x) = 1.094 \times 10^6 \frac{(1+x)^{3.231}}{44.67+x} \exp\left[-\frac{10.11}{1+x}\right] I_o,$$

$$\varepsilon_{n,\mathrm{rms}}(x) = \sqrt{1+x}\,\varepsilon_{n,\mathrm{rms}}(0). \tag{46}$$

The maximum current density technologically practical from gated field emitter arrays is likely on the order of 2000 A/cm^2: therefore, if 100 A of current is required, then the array radius would be 0.126 cm and the voltage is 206 V (corresponding to $x=0.279$ and a per-tip current of 106 μA for the active tips). The value of $\varepsilon_{n,\mathrm{rms}}(0)$ is crudely obtained by scaling using $\varepsilon'/\varepsilon=(L'/L)\sqrt{V/V'}$: taking $L'=\sqrt{\pi\rho_c}$, $V'=V(0)$, and $\varepsilon=23$ mm mrad, then $\varepsilon_{n,\mathrm{rms}}(0)=12.8$ mm mrad. The theoretical emittance of a FEA is larger than for thermionic or photocathodes. The demands per emitter may increase if pulse lengths of 10–50 ps from a FEA are required.

Issues of gated geometries and space charge

Useful field emission from metals requires fields in excess of 5 GV/m at the emission site, whereas fields in a rf photoinjector are generally on the order of 10–100 MV/m: freestanding tips would have to have field enhancement factors on the order of 100–1000. Such enhancement would be exceptional for metallic field emitters: an ellipsoidal height to base radius ratio R of 16–62 would be required based on an ellipsoidal enhancement factor given by [Eq. (92a) of Ref. 53]

$$\left.\frac{F_{\mathrm{tip}}}{F_o}\right|_{\mathrm{ellipsoid}} \approx \frac{2R^2-3}{2[\ln(2R)-1]}. \tag{47}$$

Even if possible, obtaining uniform emission from wirelike structures is difficult because of variation in field enhancement factors.[54] To improve uniformity, emitters are "conditioned" in which emitters with the largest field enhancements are degraded until their values are more representative of the group.[32,51] Applications requiring not only high current but also fast switching capability have therefore used gated FEAs.[38,55,56] The gate has advantageous and potentially problematic aspects: while the emitted beam is focused,[26,57] the high current density implies space charge effects, and beam gating implies switching time issues related to the FEA circuit's *RLC* characteristics.[58,59] A brief and qualitative discussion of the impact of each is given.

The gate and divergence of the beam

The magnitude of gate focusing can be estimated by considering the Saturn model[60,61] of a gated FEA, in which the emitter tip is replaced by a sphere holding a charge Q_s, the gate by a coplanar charged ring of radius a_g and of equal and opposite total charge $-Q_s$, and the gate-anode field by a constant background field F_o. The Saturn potential energy is given by (in spherical coordinates centered on the tip)

$$\phi_{\mathrm{Saturn}}(r,\theta) = -F_o r\cos\theta + \frac{qQ_s}{4\pi\varepsilon_0}\left\{\frac{1}{r} - \frac{1}{r_>}\sum_{j=0}^{\infty}(-1)^j\frac{(2j)!}{2^{2j}(j!)^2}\left(\frac{r_<}{r_>}\right)^{2j}P_{2j}(\cos\theta)\right\}, \tag{48}$$

where $P_j(x)$ is a Legendre polynomial, and where $r_<$ is the smaller of r or a_g, and $r_>$ the larger. To leading order in $(r_</r_>)^2$, the force in the direction $\hat{\rho}$ acting on an emitted electron is given by

$$\hat{\rho}\cdot\vec{\nabla}\,\phi_{\mathrm{Saturn}}|_{r<a} \approx \frac{qQ_s}{4\pi\varepsilon_0 r^2}\left[1-\frac{1}{2}\left(\frac{r}{a_g}\right)^3\right]\sin\theta,$$

$$\hat{\rho}\cdot\vec{\nabla}\,\phi_{\mathrm{Saturn}}|_{r>a} \approx -\frac{3a_g^2 qQ_s}{4\pi\varepsilon_0 r^4}\sin\theta, \tag{49}$$

where $r^2=z^2+\rho^2$ (all terms of which are dimensioned) and $\tan\theta=\rho/z$. The presence of the second term in parentheses (the "gate" term) is therefore seen to give rise to a force opposing an axial expansion of the beam both within the unit cell ($r<a$) and away from it ($r>a$). That is, the beam is more collimated. However, the axial force component will both reduce the magnitude of the γ's and C, thereby mitigating the impact, in line with the arguments of O'Shea[8] that an electrostatic focusing structure will not reduce the emittance—or, alternately, the beam is already at a waist within the unit cell.

Impact of space charge: An estimate

For high current operation, space charge effects will expand the beam and the question is how the magnitude of space charge forces within the unit cell compares with fields therein. For a crude estimate, assume that the apex field F_{tip} is generated solely by Q_s. Using the parameter characteristic of the field emitter corresponding to line F1 in Fig. 6 for a current of 10 μA, $Q_s=4\pi\varepsilon_0 a_{\mathrm{tip}}^2 F_{\mathrm{tip}}/q\approx 469q$. Compare this to the charge ΔQ existing within the hemisphere over the tip-gate region, approximated by

$$\Delta Q = \int I_{\mathrm{tip}}dt \approx \int_0^{a_g}\frac{I_{\mathrm{tip}}}{\nu(z)}dz < \frac{mI_{\mathrm{tip}}}{\hbar k_F}a_g. \tag{50}$$

Assuming $I_{\mathrm{tip}}=10$ μA and Table IV parameters, $\Delta Q=16.2q$. Higher current per tip will commensurately increase ΔQ but it is clear that unless the individual emitters are driven on the order of 0.3 mA or harder, Q_s will tend to dominate ΔQ, that is, the influence of the gate exceeds the influence of the space charge within the unit cell. Therefore, the emittance formula of Eq. (32) is approximately correct.

The gate and switching time

A thermionic source is run space-charge limited for which the current varies as a power (3/2) of the grid voltage, so that the grid voltage must be reduced almost to vanishing to turn off the beam. In contrast, field emission current varies exponentially with gate voltage so that reducing the gate voltage by a fraction of its peak value suffices.[53,59] Consider the consequences of generating a nanocoulomb charge bunch in 50 ps from a source required to turn off completely in 10 ps. The questions are: what constitutes "complete turn-off" and what consequences arise by insisting on a switching time of 10 ps?

First, let σ be the ratio between the minimum and maximum currents. Then the minimum voltage is the $n\gg 1$ limit of the recursion relation,

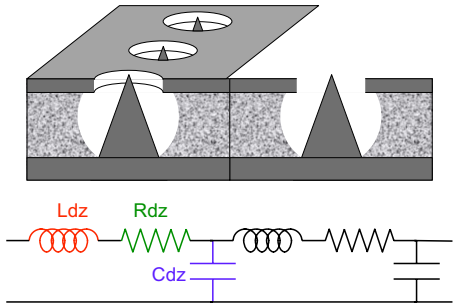

FIG. 8. (Color online) *RLC* circuit used to model a FEA for the evaluation of the array length maximum.

$$V_{n+1} \approx \frac{BV_n}{B + V_{\max} \ln\left[\frac{1}{\sigma}\left(\frac{V_n}{V_{\max}}\right)^2\right]}. \tag{51}$$

With $V_0 \approx V_{\max}$, convergence is achieved to better than 1% after six iterations. We find $V_{\min}/V_{\max}=71.8\%$ for $\sigma=0.01$ and 49.9% for $\sigma=10^{-5}$, an advantage in reducing the drive power required to modulate a gate.[59] In short, the "extinction ratio" is excellent.

Second, a FEA may be represented as a bunch of coupled *RLC* units.[58,59,62,63] The analysis follows that of Murphy and Kodis[59] to analyze the circuit suggested by Fig. 8 and therefore uses their notation. The inductance L, the resistance R, and the capacitance C are per unit length, and z is the direction in which the signal causing the gate potentials to shift is propagating. Let the gate current and potential be denoted by I_g and V_g, respectively. Further, let the sinusoidal frequency of the gate be ω with the consequence that the $I_g[V_g^{\rm dc}+V_g^{\rm rf}\cos(\omega t)]$ curve can be made to resemble a sequence of well-spaced pulses by adjusting the ratio of $B/V_{\max}$ to a number of order of 10. Using $I_g^{\rm rf}(z,t) = \mathrm{Re}[\tilde{I}_g(z)e^{i\omega t}]$ and analogously for V, the transmission line equations

$$\partial_z \tilde{I}_g(z) = -i\omega C\tilde{V}_g(z),$$

$$\partial_z \tilde{V}_g(z) = -(R+i\omega L)\tilde{I}_g(z) \tag{52}$$

result and have solutions $\tilde{I}_g(z)=(-iV_o/Z_o)\sin(\beta z)$ and $\tilde{V}_g(z) = V_o\cos(\beta z)$, where

$$\beta \equiv \omega\sqrt{LC}\left[1 - i\frac{R}{\omega L}\right]^{1/2},$$

$$Z_o \equiv \omega\sqrt{\frac{L}{C}}\left[1 - i\frac{R}{\omega L}\right]^{1/2}. \tag{53}$$

Equation (52) demonstrates that the gate voltage for each emitter row changes with z, and the emitted current changes along the rows away from where the input signal is fed into the array. If an array of width w and length l is to emit uniformly, then $|\beta l| \ll 1$. Evaluating the l that satisfies the inequality requires estimates of R, L, and C for the unit cell.

The *RLC* unit cell characterization of a FEA of Calame *et al.*[58] benefits from a sequence of approximations that allow for scaling arguments to be employed.[35] Let s be the scale factor such that $s=1$ corresponds to dimensions the in Table II: $s=2$ would be twice as large, etc. The gate radius, tip-to-tip separation, base-to-gate separation, and gate layer thickness all scale linearly with s. The apex radius, work function, and cone angle in contrast are held fixed regardless of scale size. As per Ref. 35 the following scalings follow:

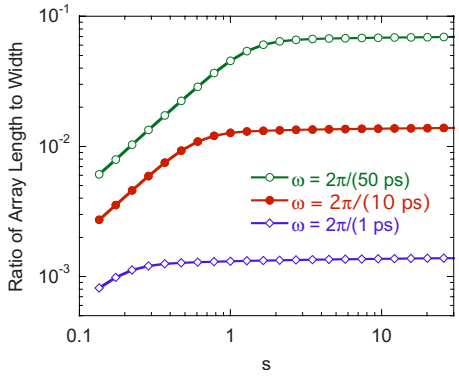

FIG. 9. (Color online) Variation of the ratio (l/w), as per Eq. (60); as a function of array scaling factor s for three different switching speeds (50, 10, and 1 ps), showing that the slower the switching speed, the greater the length of the array can be.

$$\beta_g\left(\frac{q}{\rm nm}\right) = 0.080\,65\left\{\frac{\pi}{\ln[55.4s(2.844+s)]} - 0.093\,47\right\}, \tag{54}$$

$$R\left(\frac{\Omega}{\rm cm}\right) = \frac{5.544}{s}, \tag{55}$$

$$L\left(\frac{\rm nH}{\rm cm}\right) = 24.19s, \tag{56}$$

$$C[\varepsilon_0] = \frac{5401}{s}\left\{1 + \frac{1.462}{\ln[55.4s(2.844+s)]}\right\}, \tag{57}$$

where $nH=10^{-9}$ H, and units are in the square brackets. Equation (57) is derived from

$$C = C_o\left[1 - \pi\left(\frac{a_g}{d_{tt}}\right)^2\right] + (C_{ec}+C_{er})\frac{w}{d_{tt}^2}, \tag{58}$$

assuming that ring and cone capacitances scale as [see Eq. (11b) of Ref. 35]

$$C_o[\varepsilon_0] = \frac{3125}{s},$$

$$C_{er}[\varepsilon_0\mu\mathrm{m}] = 70.12s\beta_g(s),$$

$$C_{ec}[\varepsilon_0\mu\mathrm{m}] = 7.031s. \tag{59}$$

Defining $p \equiv |\beta l|$, it follows

$$\frac{l}{w} = \frac{p}{\{\omega^2C^2[R^2+\omega^2L^2]\}^{1/4}}. \tag{60}$$

For $p=0.1$, the dependence of Eq. (60) is shown in Fig. 9 for several values of frequency related to the inverse rise time, taken to be 50, 10, and 1 ps, respectively.

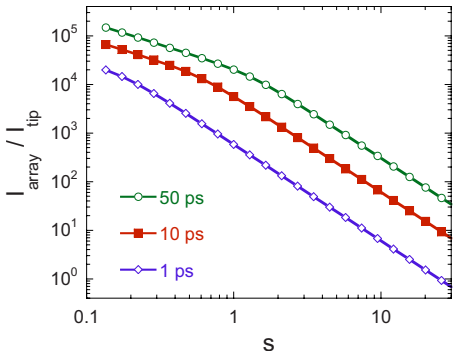

FIG. 10. (Color online) Ratio of array current to single tip current calculated by Eq. (61) as a function of array scaling factor s. Smaller emitters (small s) need not be driven as hard individually (large ratio) for a given total current.

The value of l relates to how hard the tips must be driven for a desired current. Letting the tip current be given by Eq. (37), the array current is

$$I_{\text{array}}(V) = I_{\text{tip}}(V)\left(\frac{lw}{d_{tt}^2}\right). \tag{61}$$

Given that w/d_{tt} scales as $666.7/s$, then the ratio of array current to tip current is shown in Fig. 10. For the 10 ps line, if each tip is driven no harder than 0.1 mA/tip and the array current is $(1\ \text{nC})/(50\ \text{ps}) = 20$ A, then $I_{\text{array}}/I_{\text{tip}}$ would have to be at least 2×10^5, which is not met (for the value $s=1$, the ratio is a factor of 10 too small). Consequently, the packing density, work function, array width w, or rise/fall time, and possibly all, would have to increase/decrease according to their impact.

CONCLUSION

Formulas for the emittance of a field emission structure similar in simplicity to those of thermal and photoemission have been absent due to the complications introduced by multidimensionality. This work reports such formulas for flat, single tip, and array configurations. First, a planar field emission emittance equation was developed for 1D geometries. Second, the consequences of an array of emitters was developed. Third, a PCM was developed to obtain the initial coordinates of emitted electrons and their relative proportion as a function of location on the emitter apex. Fourth, the method by which the trajectories gave parameters needed in the developed formula for emittance from an array was presented. When applied to Spindt-type emitters, the model predicts that the emittance of a square array of 0.2 cm on a side of ungated molybdenum emitters to be 23 mm mrad.

Other comparisons were made. First, thermal, photo, and field emission sources were compared. Second, the magnitude of space charge expansion forces within the unit cell was shown to be less than the influence of the gate and shall be taken up in a separate study. Third, the requirement that the FEA be switched on and off rapidly was related to the FEA *RLC* parameters, and constraints on the field emitter length were found, showing that switching the arrays in under 10 ps for performance conditions of interest herein may be challenging.

ACKNOWLEDGMENTS

We gratefully acknowledge support provided by the Naval Research Laboratory, the Office of Naval Research and the Joint Technology Office. We also thank C. Brau (Vanderbilt University) for suggestions resulting in the manuscript's improvement.

[1] J. W. Lewellen, Proceedings of the IEEE Particle Accelerator Conference 2005 (IEEE, New York, 2005), p. 563.
[2] V. L. Granatstein, R. K. Parker, and C. M. Armstrong, Proc. IEEE **87**, 702 (1999).
[3] R. K. Parker, R. H. Abrams, Jr., B. G. Danly, and B. Levush, IEEE Trans. Microwave Theory Tech. **50**, 835 (2002).
[4] W. D. Jensen, F. B. Gerhard, Jr., and D. M. Koffman, in *Van Nostrand's Scientific Encyclopedia*, edited by G. D. Considine, and P. H. Kulik (Wiley, New York, 2005), p. 1771.
[5] P. Kruit, M. Bezuijen, and J. E. Barth, J. Appl. Phys. **99**, 024315 (2006).
[6] M. J. Fransen, M. H. F. Overwijk, and P. Kruit, Appl. Surf. Sci. **146**, 357 (1999).
[7] R. E. Thomas, Appl. Surf. Sci. **24**, 538 (1985).
[8] P. G. O'Shea, Phys. Rev. E **57**, 1081 (1998).
[9] K. L. Jensen, J. Appl. Phys. **102**, 024911 (2007).
[10] M. Reiser, *Theory and Design of Charged Particle Beams* (Wiley, New York, 1994).
[11] K. L. Jensen, P. G. O'Shea, D. W. Feldman, and N. A. Moody, Appl. Phys. Lett. **89**, 224103 (2006).
[12] R. L. Sheffield, E. R. Gray, and J. S. Fraser, Nucl. Instrum. Methods Phys. Res. A **272**, 222 (1988).
[13] D. W. Feldman, S. C. Bender, B. Carlsten, J. Early, R. B. Feldman, W. J. D. Johnson, A. Lumpkin, P. G. O'Shea, W. E. Stein, R. L. Sheffield, and K. Mckenna, Nucl. Instrum. Methods Phys. Res. A **304**, 224 (1991).
[14] P. Michelato, Nucl. Instrum. Methods Phys. Res. A **393**, 455 (1997).
[15] D. H. Dowell, Proc. SPIE **3614**, 14 (1999).
[16] G. R. Neil, C. Behre, S. V. Benson, M. Bevins, G. Biallas, J. Boyce, J. Coleman, L. A. Dillon-Townes, D. Douglas, H. F. Dylla, R. Evans, A. Grippo, D. Gruber, J. Gubeli, D. Hardy, C. Hernandez-Garcia, K. Jordan, M. J. Kelley, L. Merminga, J. Mammosser, W. Moore, N. Nishimori, E. Pozdeyev, J. Preble, R. Rimmer, M. Shinn, T. Siggins, C. Tennant, R. Walker, G. P. Williams, and S. Zhang, Nucl. Instrum. Methods Phys. Res. A **557**, 9 (2006).
[17] A. Todd, Nucl. Instrum. Methods Phys. Res. A **557**, 36 (2006).
[18] L. A. DuBridge, Phys. Rev. **43**, 0727 (1933).
[19] D. H. Dowell and J. F. Schmerge, Phys. Rev. ST Accel. Beams **12**, 074201 (2009).
[20] K. L. Jensen, N. A. Moody, D. W. Feldman, E. J. Montgomery, and P. G. O'Shea, J. Appl. Phys. **102**, 074902 (2007).
[21] J. F. Schmerge, J. M. Castro, J. E. Clendenin, D. H. Dowell, S. M. Gierman, and R. O. Hettel, in *Proceedings of the 26th International Free Electron Laser Conference*, (Comitato Conferenze Elettra, Trieste, Italy, 2004), pp. 205–208.
[22] E. L. Murphy and R. H. Good, Phys. Rev. **102**, 1464 (1956).
[23] R. G. Forbes, Appl. Phys. Lett. **89**, 113122 (2006).
[24] J. H. B. Deane and R. G. Forbes, J. Phys. A: Math. Theor. **41**, 395301 (2008).
[25] J. W. Gadzuk and E. W. Plummer, Rev. Mod. Phys. **45**, 487 (1973).
[26] K. L. Jensen, P. Mukhopadhyay-Phillips, E. Zaidman, K. Nguyen, M. Kodis, L. Malsawma, and C. Hor, Appl. Surf. Sci. **111**, 204 (1997).
[27] J. D. Zuber, K. L. Jensen, and T. E. Sullivan, J. Appl. Phys. **91**, 9379 (2002).
[28] K. L. Jensen, D. W. Feldman, and P. G. O'Shea, J. Vac. Sci. Technol. B **23**, 621 (2005).
[29] K. L. Jensen, Y. Y. Lau, D. W. Feldman, and P. G. O'Shea, Phys. Rev. ST Accel. Beams **11**, 081001 (2008).
[30] P. R. Schwoebel, C. A. Spindt, and C. Holland, J. Vac. Sci. Technol. B **23**, 691 (2005).
[31] M. J. Rhee and K. A. Boulais, Phys. Fluids B **3**, 1781 (1991).
[32] P. R. Schwoebel, C. A. Spindt, and C. Holland, J. Vac. Sci. Technol. B **21**, 433 (2003).
[33] R. G. Forbes and K. L. Jensen, Ultramicroscopy **89**, 17 (2001).
[34] K. L. Jensen, J. Appl. Phys. **107**, 014905 (2010).
[35] K. L. Jensen, J. Appl. Phys. **83**, 7982 (1998).
[36] K. L. Jensen and C. Marrese-Reading, J. Vac. Sci. Technol. B **21**, 412

(2003).
[37]C. Y. Hong and A. I. Akinwande, J. Vac. Sci. Technol. B **21**, 500 (2003).
[38]C. A. Spindt, C. Holland, P. R. Schwoebel, and I. Brodie, J. Vac. Sci. Technol. B **16**, 758 (1998).
[39]R. Ganter, R. J. Bakker, R. Betemps, M. Dehler, T. Gerber, J. Gobrecht, C. Gough, M. Johnson, E. Kirk, G. Knopp, F. Le-Pimpec, K. Li, M. Paraliev, M. Pedrozzi, L. Rivkin, H. Sehr, L. Schulz, and A. Wrulich, J. Vac. Sci. Technol. B **24**, 974 (2006).
[40]R. Ganter, K. Li, M. Dehler, J. Gobrecht, L. Rivkin, and A. Wrulich, J. Vac. Sci. Technol. B **23**, 680 (2005).
[41]C. H. Boulware, J. D. Jarvis, H. L. Andrews, and C. A. Brau, Int. J. Mod. Phys. A **22**, 3784 (2007).
[42]C. A. Brau, Nucl. Instrum. Methods Phys. Res. A **393**, 426 (1997).
[43]C. A. Brau, Nucl. Instrum. Methods Phys. Res. A **407**, 1 (1998).
[44]C. H. Garcia and C. A. Brau, Nucl. Instrum. Methods Phys. Res. A **475**, 559 (2001).
[45]C. H. Garcia and C. A. Brau, Nucl. Instrum. Methods Phys. Res. A **483**, 273 (2002).
[46]R. Ganter, R. Bakker, C. Gough, S. C. Leemann, M. Paraliev, M. Pedrozzi, P. Le, F. V. Schlott, L. Rivkin, and A. Wrulich, Phys. Rev. Lett. **100**, 064801 (2008).
[47]R. Ganter, R. J. Bakker, C. Gough, M. Paraliev, M. Pedrozzi, F. Le Pimpec, L. Rivkin, and A. Wrulich, Nucl. Instrum. Methods Phys. Res. A **565**, 423 (2006).
[48]J. Jarvis, Ph.D. thesis, Vanderbilt University, Nashville, TN, 2008.
[49]S. C. Leemann, A. Streun, and A. Wrulich, Phys. Rev. ST Accel. Beams **10**, 071302 (2007).
[50]D. Temple, Mater. Sci. Eng. R. **24**, 185 (1999).
[51]C. A. Spindt, I. Brodie, C. E. Holland, and P. R. Schwoebel, in *Vacuum Microelectronics*, edited by W. Zhu (Wiley, New York, 2001), p. 105.
[52]J. F. Schmerge, J. E. Clendenin, D. H. Dowell, and S. M. Gierman, Int. J. Mod. Phys. A **22**, 4069 (2007).
[53]K. L. Jensen, in *Vacuum Microelectronics*, edited by W. Zhu (Wiley, New York, 2001), p. 33.
[54]L. Nilsson, O. Groening, O. Kuettel, P. Groening, and L. Schlapbach, J. Vac. Sci. Technol. B **20**, 326 (2002).
[55]C. A. Spindt, C. Holland, P. R. Schwoebel, and I. Brodie, J. Vac. Sci. Technol. B **14**, 1986 (1996).
[56]K. L. Jensen, R. H. Abrams, and R. K. Parker, J. Vac. Sci. Technol. B **16**, 749 (1998).
[57]R. L. Hartman, W. A. Mackie, and P. R. Davis, J. Vac. Sci. Technol. B **14**, 1952 (1996).
[58]J. P. Calame, H. F. Gray, and J. L. Shaw, J. Appl. Phys. **73**, 1485 (1993).
[59]R. A. Murphy and M. A. Kodis, in *Vacuum Microelectronics*, edited by W. Zhu (Wiley, New York, 2001), p. 349.
[60]K. L. Jensen, E. Zaidman, M. Kodis, B. Goplen, and D. Smithe, J. Vac. Sci. Technol. B **14**, 1942 (1996).
[61]C.-W. Lu and C. L. Lee, IEEE Trans. Electron Devices **45**, 2238 (1998).
[62]P. M. Phillips, R. E. Neidert, L. Malsawma, and C. Hor, IEEE Trans. Electron Devices **42**, 1674 (1995).
[63]M. A. Kodis, K. L. Jensen, E. G. Zaidman, B. Goplen, and D. N. Smithe, IEEE Trans. Plasma Sci. **24**, 970 (1996).